

## A Finite Element Model to Predict Wellbore Fracture Pressure with Acid Damage (Model Unsur Terhingga untuk Meramalkan Retak Tekanan Telaga Gerudi dengan Kerosakan Asid)

FANHUI-ZENG\*, JIANCHUN-GUO & YUXUAN-LIU

### ABSTRACT

*Hydraulic fracturing becomes more difficult when confronted with a formation of high fracturing pressure. In such formations, acidizing before the main fracturing treatment provide a method to reduce fracture pressure. The aim of this paper was to investigate the evolution of fracture pressure in a wellbore with acidizing. Five experiments were conducted to study the mechanisms of acid damage on reservoir minerals and cementing materials properties. Consequently, a mathematical model to predict fracture pressure with acidizing has been established and verified by field data. The analysis results showed that it is possible to reduce fracture pressure with decreased rock strength and fracture critical stress intensity factor by means of acid damage. Acid damage destroys the crystal structure of mineral particles, breaks the crystalline layers in cementing materials, increases rock porosity and reduces the rock strength. In addition, as the acid concentration, formation temperature and acid treatment time increased, it was useful to reduce fracture pressure in the wellbore. Using the proposed model, we were able to select the optimal acid damage construction parameters to reduce fracture pressure.*

*Keywords: Acid damage; fracture pressure; hydraulic fracture; mechanisms of acid damage; prediction model*

### ABSTRAK

*Keretakan hidraulik menjadi sukar apabila berhadapan dengan pembentukan tekanan keretakan tinggi. Dalam pembentukan itu, pengasidan sebelum rawatan keretakan utama merupakan suatu kaedah bagi mengurangkan tekanan retak. Tujuan kajian ini adalah untuk mengkaji evolusi tekanan retak dalam telaga gerudi dengan pengasidan. Lima kajian telah dijalankan untuk mengkaji mekanisme kerosakan asid dalam tangki mineral dan sifat bahan penyimenan. Oleh yang demikian, model matematik untuk meramalkan tekanan retak dengan pengasidan telah dibangun dan dibuktikan melalui data lapangan. Keputusan analisis menunjukkan bahawa tekanan retak dapat dikurangkan dengan mengurangkan kekuatan batu dan faktor keamatan tekanan kritikal retak melalui kerosakan asid. Kerosakan asid memusnahkan struktur kristal zarah mineral, memecahkan lapisan kristal dalam bahan penyimenan, meningkatkan keliangan batu dan mengurangkan kekuatan batu. Sebagai tambahan, semasa kepekatan asid, suhu pembentukan dan tempoh rawatan asid meningkat, adalah disarankan tekanan retak dikurangkan dalam telaga gerudi. Berdasarkan model yang dicadangkan, kami dapat memilih parameter penghasilan kerosakan asid yang optimum untuk mengurangkan tekanan retak.*

*Kata kunci: Kerosakan asid; mekanisme kerosakan asid; model ramalan; retak hidraulik; tekanan retak*

### INTRODUCTION

Hydraulic fracturing is a key technology to develop deep and low permeability sandstone reservoirs. In several instances, fracture stimulation in production wells is likely to fail due to large *in situ* stresses, high rock strength and severe formation damages inherited from well drilling and completion. However, the most common problem with these reservoirs is the high fracture pressure of target formation. In order to solve this problem, the method of acid damage has been developed to reduce the fracture pressure. By this method, acid was injected into pay zone to react with the mud cake, solid particles, mineral particles and cementing materials, leading to the alteration of the mineral composition, particle size, rock porosity, permeability and strength and consequently reducing the formation fracture pressure. Subsequent to acid damage, accurate prediction of fracture pressure was important

for selection of suitable hydraulic fracturing equipment, including frac-string and down hole packer. In order to model the evolution of fracture pressure with acid damage, this study took two main tasks into consideration: Firstly, studying the variation of rock properties with exposure to acid and secondly, the prediction of fracture pressure under decreasing values of Young's modulus and critical stress intensity factor.

Several studies have so far been carried out on the first aspect. Hoshino (1974) conducted a sufficient amount of research, correlating the compressive strength of unconfined sandstones with their index engineering properties, such as density, absorption, moisture content, porosity and pore size distribution. A few studies have also tested the effect of fluid chemistry on the behavioral strength of geologic materials. Colback and Wild (1965) demonstrated a 50% loss in uniaxial compressive strength

from dry to saturated conditions in shale and quartzite sandstone. Wiederhorn and Johnson (1973) observed true stress corrosion in double-cantilever-beam crack and fracture propagation experiments. Sibson (1977) investigated that fluids drive the development of secondary fractures, such as joints and faults and assist the formation of near-surface fault rocks such as gouge and breccias. Atkinson (1979) studied the subcritical tensile cracking of quartz in wet environments, facilitated by the chemical reaction between the siloxane bonds of the quartz and the water or water vapour in the surrounding environment (stress corrosion). Higgs (1981) observed that the presence of water reduced the coefficient of friction to 35° using cut samples of Tennessee sandstone. Freiman (1984) observed the chemical weakening effects in glass and quartz deformed in the presence of aqueous chemical environments, which relates to hydrogen chemisorptions at the tip of a propagating crack. Hawkins and McConnell (1992) tested the loss in uniaxial compressive strength between dry and saturated samples for 35 British sandstones, being 78% for the clay-rich Cretaceous Greensand, while for the Siliceous Sandstone the strength decreased by 8%, demonstrating a large variation in sensitivity to moisture content throughout the range of sandstones. Feng et al. (2001) pointed out the fluid-related chemical processes as affected by fluid composition, in addition to extrinsic parameters such as temperature and pressure. For aqueous fluids, increasing ionic strength has been shown to reduce rock strength by facilitating the formation of micro-fractures and lowering the free energy of fracture surfaces. Niemeijer and Lloyd (2006) observed that stress corrosion can affect the strength and behavior of rocks, especially at higher temperatures, where reaction kinetics are more favorable. These studies show that rock properties do change under certain conditions. It was therefore one of the aims of this study to extend the previous research to show the changes of rock properties with acid damage.

The second important issue considered by this study was the prediction of fracture pressure in a wellbore, which has also been extensively studied by several authors. Haimson and Fairhurst (1967) investigated the fracturing pressure, taking into account the *in situ* stresses and rock properties. Eaton (1969) established a fracture prediction formula using well log data and assuming that fracture gradient changes with well depth. Anderson et al. (1973) added the influence of Biot coefficient to the prediction formula. Stephen et al. (1982) proposed a new prediction model by coupling the effects of tectonic stress. Huang and Xu (1986) presented a new model with inhomogeneous stress field. Hossain et al. (1999) presented a generic model for prediction of hydraulic fracture initiation pressure, including the orientation and location of fractures in the wellbore wall. However, the accurate prediction of well bore fracture pressure requires an accurate prediction of the stress field in the vicinity of the crack tip for the given structural geometry, loading and boundary conditions, while the analytical solutions were only available in certain

relatively simple cases due to the complicated boundary conditions associated with the governing equations. The analytical solution considers the rock as an elastic medium and assumes that the well is under plane-strain condition and the fracture pressure of the well bore is determined by equating the circumferential stress at a well surface to the tensile failure stress of the rock medium.

Some researchers have done studies related to fracture initiation and propagation by means of the finite element method (FEM), which was extensively used for the solution of practical fracture problems due to its accuracy, convenience and flexibility. Hu et al. (2003) provided a method to calculate fracture pressure in perforated wells by FEM. Asadpourea et al. (2006) provided an extended finite element method to model a crack growth in 2D orthotropic media. Besides, they have testified that the FEM was suitable for modelling and analyzing crack domain primary factors. Rajesh and Rao (2010) presented a coupling technique for integrating the element-free Galerkin method with the finite element method to analyze homogeneous, anisotropic and two dimensional linear-elastic cracked structures subjected to mixed-mode (Mode I and Mode II) loading conditions. According to the literature reviewed previously, many laboratories scaled rock strength tests with hydro-chemistry or aqueous solutions have been conducted under the circumstances of normal temperature. But, these tests did not take sufficient consideration of the condition that the HCl or HCl-HF react strongly with minerals at high temperature in a few minutes. The previous test conditions cannot be the representative of field conditions during acid damage. Until now, the model development concentrate on the prediction of well bore fracture pressure without acid damage and the model considering acid damage in particular is inaccessible. This paper was focused on filling this knowledge gap and in the first place predicting the fracture pressure.

This paper studied the damage mechanisms of minerals and cementing materials using several experiments and consequently establishes a model to predict the fracture pressure with acid damage. The model was developed with a limitation that it did not consider the leak-off and pore pressure changes in the near wellbore zone during hydraulic fracture. However, it was believed that this limitation was not essential as it did not affect the reliability of the results.

## MATERIALS AND METHODS

### SAMPLING

Sandstone is an aggregation of rocks and minerals, which essentially consists of silicates (quartz & feldspar) and clays (montmorillonite & kaolinite). In essence rock strength is the structural force generated between the mineral particles and links the force formed by the cementing materials. Because the structural strength is larger than that of cementing strength, whether it is easy or not to destroy rocks mainly depends on the cementing

strength. Studying the reaction of particles and cementing materials with acid solution is helpful to understand the mechanism of acid damage on reducing rock strength.

The mineral samples, bought from the Education Geological Specimens Factory of Yuhang District, Hangzhou, Zhejiang Province in China, have a purity of above 95%, as identified by X-ray diffraction. The core samples collected from the Western Sichuan Basin in China were dark grey brown sandstone, belonging to the group of Jurassic Shaximiao formation, from the well Xin808, which depth was 1977 m from the surface. Its porosity and permeability was 8.5% and  $6.5 \times 10^{-3} \mu\text{m}^2$ , respectively. These cores contain 37.5 wt. % quartz, 40.3 wt. % feldspar, 5.5 wt. % carbonate, 1.6 wt. % kaolinite, 3.9 wt. % chlorite, 6.0 wt. % illite and 5.2 wt. % montmorillonite, as identified by the X-ray diffraction. The formation temperature is 60°C and overburden pressure was maintained at 44.5 MPa, with a pore pressure of 23.7 MPa.

#### METHODS

In order to search for the acid damage on the rock mechanic properties, the following five experiments was conducted. The test indicated how acid damage destroyed the crystal structure of mineral particles and rock sample mechanical property.

##### ION CONCENTRATION TEST

Coarse quartz sand and feldspar was ground into a fine powder of 50-500  $\mu\text{m}$  particle size. Several 2.0 g samples of this powder were weighed off using an electronic balance and loaded into inert plastic reaction flasks. 10.0 mL of acid (5 wt. % HCl+1.0 wt. % HF, 5 wt. % HCl+0.5 wt. % HF and 5 wt. % HBF<sub>4</sub>) was added onto each sample in the flask (the solid / liquid ratio is 10 g/50 mL) and then covered with a tight fitting lid and carefully shaken into a homogenous mixture.

The flasks were then placed into a warm bath of distilled water at 60°C and left under these conditions for different reaction times (15, 30, 45 and 60 min). When the reaction time pre-set for each sample had been achieved, the flasks were removed from the warm bath and put into a desiccators and left to cool to room temperature.

The inert plastic flask was then removed from the desiccators and slightly shaken to fully mix the solid and liquid contents. 2 to 3 min were allowed for liquid clarification after shaking. A needle was used to draw off the supernatant, as a means to separate the solid and liquid phases. Silicon and aluminium concentrations in the liquid phase (supernatant) were analysed to monitor the changes in mineral structure. In this experiment, a 721B spectrophotometer was used to determine the concentration of these elements.

##### XRD EVALUATION

Cementing materials (montmorillonite & kaolinite) were ground into a fine powder of 50-500  $\mu\text{m}$  particle size.

Again several 2.0 g samples of this powder were weighed off using an electronic balance and loaded into inert plastic reaction flasks. A Phillips X-ray diffraction experiment were conducted on the residual solid to analyze the changes in mineral structure.

##### CORE FLOW TESTS

These tests were used to simulate the flow process when acid reacts with the formation rock. The experimental apparatus consists of a double-plunger micro-pump, a thermostat, 3 piston-type acid containers, a core holder, a manual pumps, flow meters, pressure pipes and other accessories. The double plunger micro-pump was used to ensure a stable output pressure or flow rate and the incubator or thermostat is used to ensure a constant system temperature.

##### TRIAxIAL COMPRESSION TESTS

Triaxial compression tests were conducted to study the influence of acid damage on rock strength. The core samples (with or without acid treat) for triaxial compression tests were loaded axially till broken at the constant confining pressure (minimal principal stress) and pore pressure. The peak value of the axial stress was considered the confining compressive strength of the sample. A U.S. GCTS's RTR-1000 triaxial rock mechanics experimental apparatus was used to measure the elastic constants of the rock samples, including the compressive strength, elastic modulus, Poisson's ratio and other mechanical parameters.

##### THIN SECTION EVALUATION

A thin section study of acid damage and undamaged cores were performed to determine the effect of various treating acid fluids on the cores structure and mineralogy. The dyed resin (red) was added into the rock pore space before and after acid damage under vacuum conditions to make liquid plastic or resin consolidation at a certain temperature and pressure. The rock sample was then cut into thin slices and a microscopic observation was performed on the two-dimensional structure associated with the pore and throat and their connections.

#### RESULTS AND DISCUSSION

The five tests described earlier yielded plenty of useful information, as discussed in this section.

Figure 1 test results indicated how acid damage destroys the crystal structure of mineral particles. Figure 1(a) shows the crystal stereo-chemical structure of quartz. It is a typical covalent compound with silicon-oxygen tetrahedrons, in which the silicon and oxygen are located in the centre and four corners of the tetrahedron, respectively. Silicon and oxygen are linked through the shared electrons to form the chemical bond. Figure 1(b) shows the elemental concentration of Si in the spent acid solutions of quartz reacted with 5 wt. % HCl+1.0 wt. % HF, 5 wt. % HCl+0.5

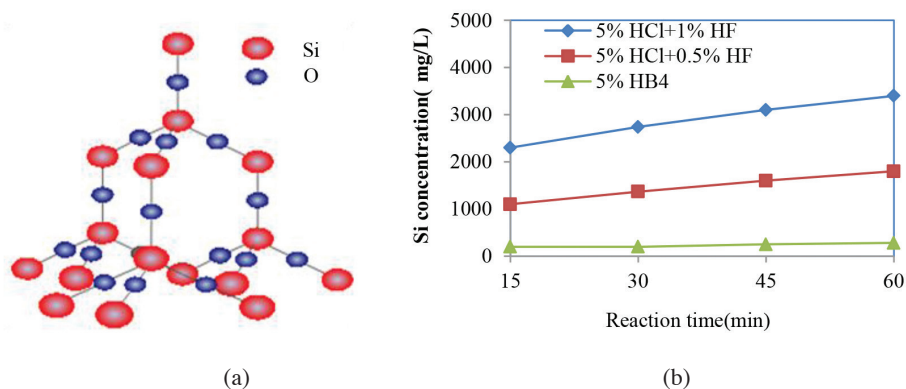


FIGURE 1. (a) Stereochemical crystal structure of quartz and (b) Variation of Si concentration with time in supernatant liquid (spent acid) after reaction of quartz with 3 different acids

wt. % HF and 5 wt. % HBF<sub>4</sub>, respectively. The selected reaction time intervals are 15, 30, 45 and 60 min. For the 3 different acid types evaluated, the concentrations of Si measured are 200, 1100 and 2300 mg/L after 15 min, respectively. The concentrations increase gradually with time and reached 280, 1800 and 3400 mg/L after 45 min of reaction. The increase of Si element with reacting time is related to release the Si element from the quartz, which implies that when quartz is dissolved in acid solutions, stress-enhanced diffusion of structurally-bound H<sup>+</sup> ions occurred and then hydrolysis of the strong silicon-oxygen bonds takes place (Atkinson 1979).

Feldspar is a tectosilicate, with four corners of its basic [SiO<sub>4</sub>]<sup>4-</sup> tetrahedron shared by another four [SiO<sub>4</sub>]<sup>4-</sup> tetrahedrons that links each oxygen atom with two silicon atoms. Silicon (aluminium)-oxygen tetrahedrons link with each other through bridging oxygen, meanwhile the tetrahedrons link with potassium, sodium, calcium through non-bridging oxygen. The structure A in Figure 2(a) shows the idealized potash feldspar frame structure, drawn perpendicular to A shaft. The structure B in Figure 2(a) depicts the idealized false fang ring, which constitutes an axis parallel to the chain of silica. Figure 2(b) shows the Si element concentration in spent acid solutions for 3 different reaction mixtures and time, i.e. 5 wt. % HCl+1 wt. % HF, 5 wt. % HCl+0.5 wt. % HF and 5

wt. % HBF<sub>4</sub> with feldspar. As before, the selected reaction time intervals were 15, 30, 45 and 60 min. For the 3 different reaction mixtures, the Si element concentrations measured are 570, 1730 and 2520 mg/L after 15 min. The Si element concentrations increase gradually with time and reach 1130, 2640 and 3620 mg/L after 60 min. The reaction of acid with feldspar mainly occurs at the bridging oxygen and the non-bridging oxygen, which breaks the bridging oxygen and the non-bridging oxygen, resulting in the hydroxylation of the feldspar crystal surface and the destruction of the crystal structure (Fogler 1975).

Figure 3 shows the XRD analysis of acid damage breaks the crystalline layers of the cementing materials. Montmorillonite has a layered crystal structure composed of two layers of SiO<sub>4</sub> tetrahedra interposed with a sheet layer of Al<sup>3+</sup> ions in octahedral coordination with oxygen or hydroxyl ions. Very often there will be either substitution of Al<sup>3+</sup> ion for Si<sup>4+</sup> ion in the tetrahedral layers or Mg<sup>2+</sup> and Fe<sup>2+</sup> ions for Al<sup>3+</sup> ion in the octahedral, gibbsite-type layer. These substitutions bring about a deficiency of positive charges on the composite sheet, causing a necessity for interlayer cations. These crystalline layers upgrade along the C-axis to form, for instance, a montmorillonite clay lattice. Kaolinite, on the other hand was composed of single layers of SiO<sub>4</sub>

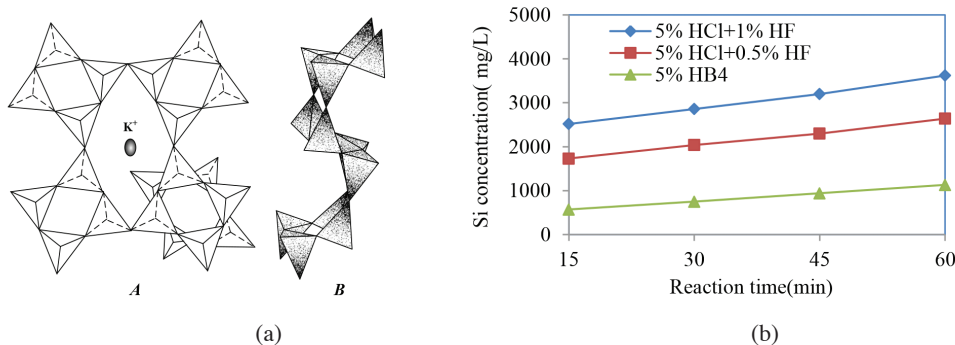


FIGURE 2. (a) Crystal structure of feldspar and (b) variation of Si concentration with time in supernatant liquid (spent acid) after reaction of feldspar with 3 different acids

tetrahedron and  $(Al_2OH_6)$  octahedron, which superpose each other. The kaolinite clay lattice was formed by these crystalline layers upgrading in the direction of *c*-axis. The forces holding the crystalline layers of kaolinite together are hydrogen bond, mainly the weak van der Waals forces and the forces within the crystalline unit are covalent bond forces. The interior of the crystalline layer was very strong, but the connection between these layers is weak and the strength is very low. Figure 3(a) and 3(b) shows the diffraction curves of Montmorillonite and Kaolinite, respectively, obtained from the solid residues after 2 h of reaction for the following mixtures: 5 wt. % HCl+1.0 wt. % HF, 5 wt. % HCl+0.5 wt. % HF and 5 wt. %  $HBF_4$ . This figure shows that the intensity of the diffraction peaks significantly decreases with the increasing strength/concentration of the acid, which implies that the layered crystalline structures of montmorillonite and kaolinite were destroyed and that the interlayer forces between the layers rendered weak by the acid.

The two tests in Figure 4 show that acid damage increases the rock porosity. Figures 4(a) and 4(b) shows the photographs of the thin-sections of the core material prior to and following the pre-flush 10 wt. % HCl and the mud acid (10 wt. % HCl+1 wt. % HF) treatment. In the untreated plate Figure 4(a), significant amounts of

quartz, potassium feldspar (microcline) and clay minerals (including elite, chlorite & illite/montmorillonite) can be observed in the compact rock. In the treated plate Figure 4(b), however, only the resistant framework mineral grains, including quartz, potassium feldspar (microcline) and some little clay minerals, can be seen with an increased uniform distribution of porosity. This implies that the HCl pre-flush and mud acid treatment effectively removed the elite, chlorite and illite/montmorillonite mixed-layer clays by dissolution to create a larger well connected porosity for fluid flow.

Table 1 shows the results obtained for the mechanical rock strength and flow parameters during core flow and tri-axial compression tests on acid treated and untreated rock samples. Core flow test condition is that each sample was first treated with 10 wt. % HCl for 10 min and then followed by a further treatment of 10-18 wt. % HCl+1-3 wt. % HF for 110 min at a constant flow rate of 5 mL/min and a constant temperature of 60°C. Tri-axial compression test conditions include a constant pore pressure of 25 MPa and the confining pressures of 40, 50 and 60 MPa. The results showed that the compressive strength, elastic modulus, internal friction angle and cohesion decrease with increasing dosage of acid for the treated core sample. Poisson's ratio shows little or no change whatever level of acid dosage used for core

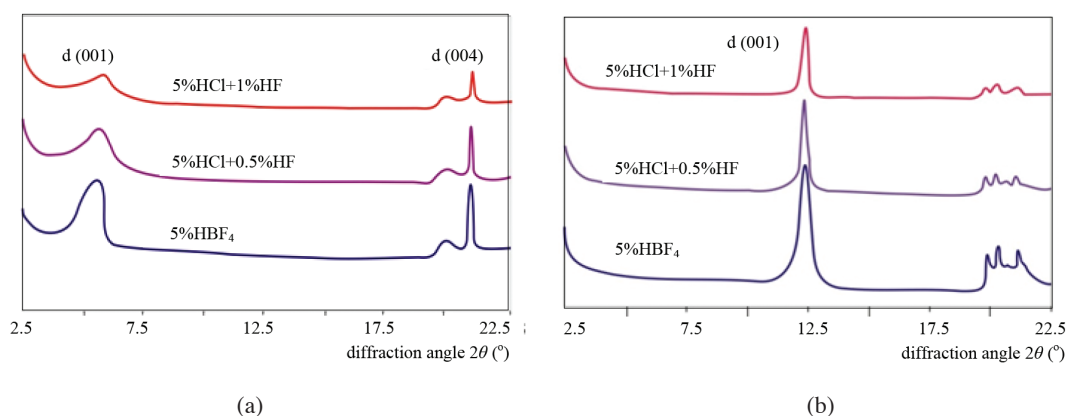


FIGURE 3. XRD diffraction curves for the clay minerals (a) Montmorillonite in the spent acid solutions and (b) Kaolinite in the spent acid solutions

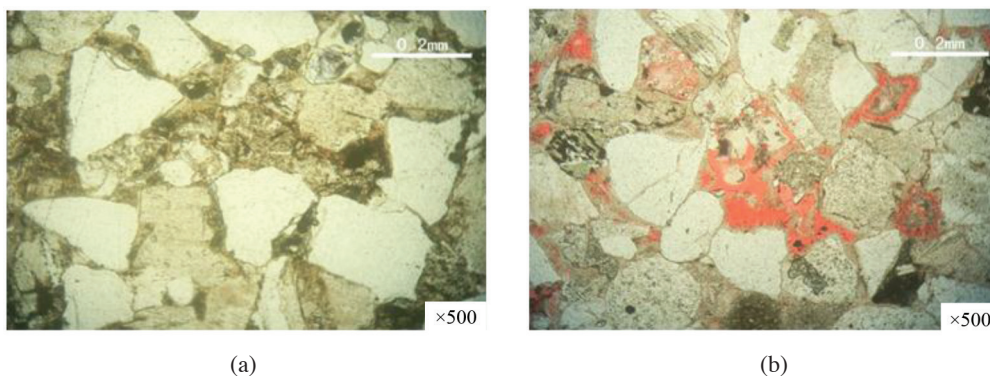


FIGURE 4. Thin-section photographs showing what the physical results of acid damage can be on the reservoir rock material

TABLE 1. The effects of acid damage on rock strength

Acid type for sample treatment	Compressive strength (MPa)	Young's modulus (MPa)	Poisson's ratio	Internal friction angle(o)	Cohesion (MPa)	Porosity (%)	Permeability ( $10^{-3}\mu\text{m}^2$ )
Untreated sample	268	35 000	0.230	24	45	8.9	6.5
10 wt. % HCl	237	32 654	0.229	20	34	11.7	12.3
10 wt. % HCl							
10 wt. % HCl+1 wt. % HF	233	30 557	0.226	18	27	14.9	15.4
10 wt. % HCl							
15 wt. % HCl+3 wt. % HF	225	29 753	0.234	18	26	17.3	20.3
10 wt. % HCl							
18 wt. % HCl+5 wt. % HF	219	27 691	0.227	16	26	20.8	24.8

treatment. On the other hand, porosity and permeability increases with increasing dosage, because the degree of erosion for the clay mineral particles, cementing materials and some other soluble minerals in sample increases with the strength/dosage of acid. The rock strength reduces due to both mechanical effects (i.e. decreasing effective stress) and chemical effects, such as hydrolytic weakening (Kronenberg et al. 1994) or stress corrosion (Atkinson 1979).

#### PHYSICAL MODELING

After the acid damage, the strength of the rock around perforations will be reduced. In order to predict the fracture pressure after the acid damage, damage mechanics and fracture mechanics need to be combined to solve the problem. This was because when the degree of damage in the zone around the perforations increases to the damage threshold, it meant the failure of rock occurred at the perforation hole, but did not mean that the perforation hole has reached an unstable state. With the development of damage, breakage will occur without delay. On the other hand, fracture mechanics can be used to determine whether the occurrence of perforations cause instability. It was necessary to combine the two different, but relative mechanics to determine fracture pressure with acid damage in perforated wells.

#### DAMAGE VARIABLE

Choosing an appropriate variable to describe reservoir material damage as a result of acid treatment was very important. Material damage will cause changes of the microstructure, including the macroscopic physical properties of the reservoir. The commonly used variables to describe acid damage include micro-cracks or pore numbers, pore lengths and pore area. Based on the results of lamella observations, acid dissolution of rock minerals will increase the number and size of micro-holes or pores in the material, thereby reducing the effective bearing area (Figure 4). Considering the observed corrosion of mineral particles and cementing materials after treatment, acid damage mainly helps to augment the size of the microspores and pores causing a reduction of the effective bearing area of the material, which was in this case defined here as a damage variable. In order to investigate the magnitude of this damage variable, an ideal cylinder of homogeneous mineral penetrating the whole length of core whose corrosion starts from the boundary toward the centre is assumed (Figure 5).

#### FRACTURE PRESSURE PREDICTION MODEL

Considering the dimension of wellbore to be much smaller in the axial than in the radial direction, the physical model

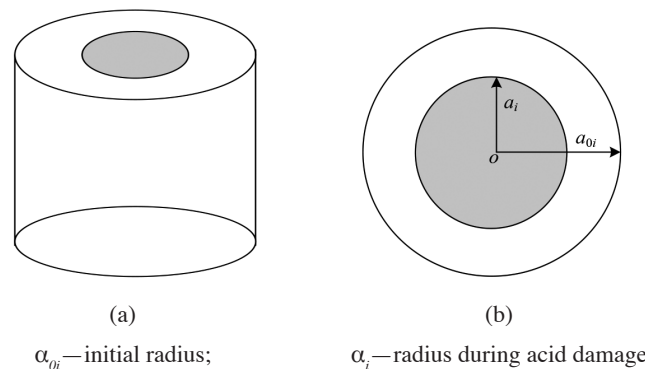


FIGURE 5. (a) Physical model of monomineralic cylinder and (b) bird's-eye view of a monomineralic core during acid damage

(Figure 6) for fracture pressure prediction with FEM can be simplified as plane strain. Let the dimension of the simulated formation be 3000×6000 mm, with perforations length and radius of 600 and 2.5 mm, respectively.

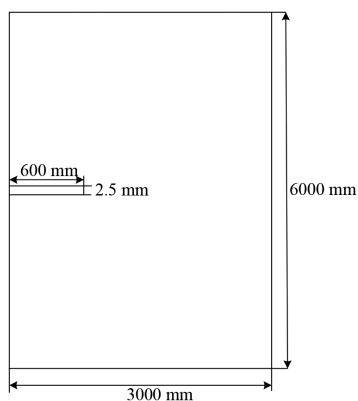


FIGURE 6. Sketch map of a perforation well

#### MATHEMATICAL MODELING DAMAGE VARIABLE MODEL

In order to set up the mathematical model, the basically assumptions made as follows:-

Sandstone was homogeneous and isotropic; Sandstone was mainly composed of quartz, feldspar, clay and carbonates and these minerals are uniformly distributed in the rock; The pad acid was HCl to fully dissolve the carbonate and the main acid was HCl + HF to dissolve aluminium silicate; The acid was injected at a constant rate. The reaction between the main acid and feldspar, quartz, clay minerals was instantaneous. Only the primary reaction of hydrofluoric acid and clay mineral was considered in the process; and The same mineral was considered as a small cylinder through the entire core. The dissolution of minerals starts from the boundary of the cylinder and gradually to the centre, which resulted in reduction of the effective bearing area (Figure 6).

As shown in Figure 5, corrosion of the rock samples lead to an increase in the porosity and consequently a decrease of the effective bearing area. The damage variable  $S_t$  after time  $t$  of reaction is defined as follows:

$$S_t = (A_{to} - A_t) / A_{to} = 1 - A_t / A_{to}, \quad (1)$$

where  $S_t$  is the damage variable, dimensionless;  $A_{to}$  is the initial bearing area,  $\text{cm}^2$ ; and  $A_t$  is the bearing area at any time  $t$ ,  $\text{cm}^2$ .

The relationship between the rate of reduction of the cylinder cross-section area and the rate of acid-rock reaction is given by (2):

$$\pi \frac{d}{dt}(a_i^2) = \frac{2\pi\alpha_i\gamma_i\beta_i M_i}{\rho_i}, \quad (2)$$

where  $a_i$  is the radius of the  $i$ th single mineral cylinder at any time, cm;  $t$  is the reaction time, s;  $\gamma_i$  is the reaction rate of acid-mineral which has been given by Fogler (1975),

Hill (1981), Kline and Fogler (1981) and William et al. (1981);  $\beta_i$  is dissolved volume of the  $i$ th homogeneous mineral with unit volume of acid composition,  $\text{m}^3/\text{m}^3$ ;  $M_i$  is the molar mass of the  $i$ th single mineral, g/mol; and  $\rho_i$  is the density of the  $i$ th single mineral in rock samples,  $\text{g}/\text{cm}^3$ .

The reaction was coupled with the following initial conditions:

$$t = 0, a_i = a_{oi},$$

where  $a_{oi}$  is the initial radius of the  $i$ th homogeneous mineral cylinder; cm and;  $a_i$  is the radius of the  $i$ th monomineralic cylinder section at any time:

$$a_i = b_i\gamma_i M_i t / \rho_i + a_{oi}, \quad (3)$$

where

$$a_{oi} = (d/2)\sqrt{(\rho/\rho_i) \times w_i}, \quad (4)$$

where  $d$  is the cylinder diameter of core sample, cm;  $\rho$  is the density of rock sample,  $\text{g}/\text{cm}^3$ ;  $\rho_i$  is the density of the  $i$ th single mineral in rock samples,  $\text{g}/\text{cm}^3$ ; and  $w_i$  is the contents of the  $i$ th single mineral in rock samples, %.

Hence, the change of the  $i$ th monomineralic cylinder section area  $\Delta A_i$ , at time can be obtained by (5):

$$\Delta A_i = \pi(a_{oi}^2 - a_i^2). \quad (5)$$

Therefore, the damage variable for the whole cylinder at any time  $t$  is obtained by (6):

$$S_t = \sum_{i=1}^n \Delta A_i / A. \quad (6)$$

According to the test conditions in Table 1, the core samples were put into database and used to calculate the change in damage variable at any time of observation by method of (5). In addition, the test results obtained for the damage variable in this paper can be compared or verified with the calculated results from the  $P$ -wave experiment by Ding and Feng (2005) (Figure 7).

This figure shows the results of the damage variable calculated from the prediction model as compared with

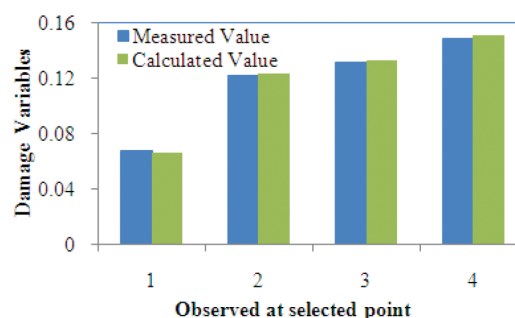


FIGURE 7. Comparison of the calculated and measured damage variables

those obtained from measuring. The chart data at the selected observation points 1, 2, 3 and 4 were the measured and calculated results for cores treated with 10 wt. % HCl pre-flush for 10 min, followed by 10 wt. % HCl+1 wt. % HF for 20, 60 and 110 min, with constant flow rates of 5 mL/min. The results of the measured damage variables were 0.06732, 0.12215, 0.13179 and 0.1483 and the corresponding modelled results were 0.06657, 0.12263, 0.13289 and 0.15024, which gave an average relative error of 0.9054%. The diagram shows a good match of the two results, implying the measured results in this paper are reasonably good.

Furthermore, a match between the damage variables calculated in (5) and the compressive strength shown in Table 1 and the relationship between the damage variable and the rock dimensionless compressive strength can be obtained using (7):

$$\sigma_{cs} / \sigma_c = 3.5854S_i^2 - 1.5429S_i + 0.9927, \quad (7)$$

where  $\sigma_{cs}$  is compressive strength of rock with acid damage, MPa; and  $\sigma_c$  is the initial compressive strength of rock before acid damage, MPa.

This equation will be used to calculate the critical stress intensity factor ( $K_{Ic}$ ).

#### FRACTURE PRESSURE MODEL

Considering the size of the drilling hole is much smaller than the axial dimension of the formation, based on the theory of rock mechanics and elasto-plastic, fracture pressure prediction can be simplified as a plane strain problem. Finite element method can therefore be used to solve the problem.

#### MATHEMATICAL MODEL WITHOUT ACID DAMAGE

The basic equations engaged include the balance equations, geometric equations and physics equations.

#### BALANCE EQUATIONS

Equilibrium differential equation

$$\begin{cases} \frac{\partial \sigma_x}{\partial x} + \frac{\partial \tau_{yx}}{\partial y} + X = 0 \\ \frac{\partial \sigma_y}{\partial y} + \frac{\partial \tau_{xy}}{\partial x} + Y = 0 \end{cases}, \quad (8)$$

where  $\sigma_x, \sigma_y$  is normal stress in  $x, y$  direction, respectively, MPa;  $\tau_{xy}, \tau_{yx}$  is shear stress in  $xy, yx$  direction, respectively, MPa;  $X, Y$  is volume force, MPa.

Static boundary conditions

$$\begin{cases} l(\sigma_x)_s + m(\tau_{yx})_s = \bar{X} \\ m(\sigma_y)_s + l(\tau_{xy})_s = \bar{Y} \end{cases}, \quad (9)$$

where  $l, m$  is integrated power direction in  $l, m$  appointed direction;  $\bar{X}, \bar{Y}$  is external force, MPa.

#### GEOMETRIC EQUATIONS

$$\{\varepsilon\} = \begin{Bmatrix} \varepsilon_x \\ \varepsilon_y \\ \gamma_{xy} \end{Bmatrix} = \begin{Bmatrix} \partial u / \partial x \\ \partial v / \partial y \\ \partial u / \partial x + \partial v / \partial y \end{Bmatrix}, \quad (10)$$

where  $\varepsilon$  is total strain, dimensionless;  $\varepsilon_x, \varepsilon_y$  are normal strain in  $x, y$  direction, respectively, dimensionless;  $\gamma_{xy}$  is shear strain, dimensionless; and  $\partial u / \partial x, \partial v / \partial y, \partial u / \partial x + \partial v / \partial y$  is the amount of deformation along  $x, y$  and total.

#### PHYSICA EQUATIONS

$$\begin{cases} \varepsilon_x = \frac{1}{E} [\sigma_x - \mu(\sigma_y + \sigma_z)] & (a) \\ \varepsilon_y = \frac{1}{E} [\sigma_y - \mu(\sigma_x + \sigma_z)] & (b) \\ \varepsilon_z = \frac{1}{E} [\sigma_z - \mu(\sigma_x + \sigma_y)] & (c) \\ \varepsilon_{xy} = \frac{1}{G} \tau_{xy} & (d) \\ \varepsilon_{yx} = \frac{1}{G} \tau_{yx} & (e) \\ \varepsilon_{zx} = \frac{1}{G} \tau_{zx} & (f) \end{cases}, \quad (11)$$

where  $E$  is young's module, MPa;  $\mu$  is Poisson's ratio, dimensionless;  $\varepsilon_z$  is the normal strain in the  $z$  direction;  $\sigma_z$  is the normal stress in the  $z$  direction, MPa;  $G$  is shear modulus, MPa;  $\gamma_{xy}, \gamma_{yz}, \gamma_{zx}$  are the shear strain in  $xy, yz$  and  $zx$  directions, respectively, dimensionless;  $\tau_{xy}, \tau_{yx}, \tau_{zx}$  are the shear stress in  $xy, yx$  and  $zx$  directions, respectively, MPa.

In plane strain state, the strain in the  $z$  direction is zero ( $\varepsilon_z = 0$ ), thus 11(c) could be reduced to:

$$\sigma_z = \mu(\sigma_x + \sigma_y). \quad (12)$$

Substituting (12) into (11) results

$$\begin{cases} \varepsilon_x = \frac{1-\mu^2}{E} \left[ \sigma_x - \frac{\mu}{1-\mu} \sigma_y \right] \\ \varepsilon_y = \frac{1-\mu^2}{E} \left[ \sigma_y - \frac{\mu}{1-\mu} \sigma_x \right] \\ \gamma_{xy} = \frac{2(1+\mu)}{E} \tau_{xy} \end{cases}. \quad (13)$$

Written in matrix form:

$$\{\sigma\} = [D]\{\varepsilon\}, \quad (14)$$

where  $[D]$  is constitutive matrix without damage, which can be represented as,

$$[D] = \frac{E(1-\mu)}{(1+\mu)(1-2\mu)} \begin{bmatrix} 1 & \frac{\mu}{1-\mu} & 0 \\ \frac{\mu}{1-\mu} & 1 & 0 \\ 0 & 0 & \frac{1-2\mu}{2(1-\mu)} \end{bmatrix}. \quad (15)$$

Equations (8) to (15) form the basic equations for a plane strain problem. These were 8 equations, including 2 boundary conditions. Unknown functions include 3 stress components ( $\sigma_x, \sigma_y, \tau_{xy}$ ), 3 strain components ( $\epsilon_x, \epsilon_y, \gamma_{xy}$ ) and 2 displacement components ( $u, v$ ). The finite element method was required to solve the problem with complex boundary and complex external load.

#### MATHEMATICAL MODEL WITH ACID DAMAGE

Under the conditions of acid damage, the damage characteristics of the material must be considered in the constitutive equation, which means the damage parameters need to be included. Compared with the fracture pressure in a wellbore without acid damage, the reduction of the fracture pressure can be exhibited by the reduction of the magnitude of the mechanical parameters (i.e. Young's modulus) and the critical stress intensity factors. Therefore the two parameters for the rock with acid damage can be calculated first as follows:

#### YOUNG'S MODULUS

Based on the strain equivalence theory (Lemaitre 1972), the relationship between constitutive matrix ( $D^*$ ) with damage and constitutive matrix ( $D$ ) without damage is defined as:

$$D^* = (1 - S_f) D, \quad (16)$$

where  $D^*$  is constitutive matrix with damage.

According to the strain equivalence theory, Poisson's ratio remains constant with and without damage. For a given damage variable, Young's modulus ( $E$ ) in a rock after acid damage can be calculated using (15) and (16).

#### CRITICAL STRESS INTENSITY FACTOR

Tang et al. (2002) have conducted a great number of research studies correlating hydration effects with  $K_{IC}$  and concluded that the critical stress intensity factor of fracture was significantly reduced with acid damage and that the degree of reduction was related to the extent of acid-rock reaction. Chen et al. (1997) have investigated the behaviour of  $K_{IC}$  in sandstone and siltstone, including the relationship between  $K_{IC}$  and the tensile strength and compression strength with acid damage ( $\sigma_{cs}$ ):

$$K_{IC} = 0.0059\sigma_t^3 + 0.0923\sigma_t^2 + 0.517\sigma_t - 0.3322, \quad (17)$$

where  $K_{IC}$  is rock critical stress intensity factor,  $\text{MPa}\cdot\text{m}^{1/2}$ ; and the  $\sigma_t$  is the rock tensile strength, MPa.

$$\sigma_t = \sigma_{cs}/20. \quad (18)$$

$K_{IC}$  with acid damage was obtained using (7), (17) and (18).

#### FRACTURE PRESSURE PREDICTION MODEL

There are three types of fracture propagation criteria under plane strain condition: Type I, Type II and the Complex Type I & II. According to the shot phasing and the complicated stress state around the wellbore, the Complex Type I & II is the best judgment criterion for rock fracture. Using FEM, the calculation of stress and strain for the perforation tip, stress intensity factors of Type I and Type II can be obtained with (19).

$$K_I = \lim_{r \rightarrow 0} \sqrt{2\pi r} \sigma_\theta (\theta = 0), \quad (19a)$$

$$K_{II} = \lim_{r \rightarrow 0} \sqrt{2\pi r} \sigma_{r\theta} (\theta = 0), \quad (19b)$$

where  $K_I, K_{II}$  are stress intensity factors for fracture Type I and Type II,  $\text{MPa}\cdot\text{m}^{1/2}$ ;  $r$  is the radial distance in the polar coordinates, m;  $\theta$  is the angle in the polar coordinates, rad; and  $\sigma_{r\theta}$  is circumferential stress, MPa.

Once  $(K_I^2 + K_{II}^2) \geq K_{IC}^2$ , the formation will break down, otherwise it did not.

#### SOLUTION PROCEDURE TO THE MATHEMATICAL MODEL

Establish the type and the content of rock sample by X-ray diffraction and calculate the initial radius for a homogeneous mineral cylinder  $a_{0i}$ ; Test the rock mechanical parameters  $E, \sigma_c$ , and  $\mu$  by triaxial compression test; Calculate the damage variable  $S_f$  in the rock for different compositions, amounts and treatment time of acid, using (6); Use the finite element method to predict the fracture pressure of wellbore; Insert data for the boundary conditions, Young's modulus ( $E$ ), Poisson's ratio ( $\mu$ ), maximum horizontal principal stress ( $\sigma_x$ ), minimum horizontal principal stress ( $\sigma_y$ ) and the fluid column pressure ( $p$ ) into the FEM model; Calculate the constitutive equation  $D^*$  for the rock with acid damage, based on (6) and (16); Calculate  $K_{IC}$ , based on Steps (2) and (3); and Calculate the stress and strain at the perforation tip based on Steps (4) to (6) and the stress intensity factor  $(K_I^2 + K_{II}^2)$  according to (19). If  $(K_I^2 + K_{II}^2) \geq K_{IC}^2$ , the formation will break down and the breakdown pressure ( $p_i$ ) equals the fluid column pressure ( $p$ ), i.e.  $p_i = p$ . Otherwise increasing  $p$  and repeats Steps (4) to (8) until  $(K_I^2 + K_{II}^2) \geq K_{IC}^2$ .

#### RESULTS AND DISCUSSION

Using the finite element method, numerical simulations were performed to investigate the effects of various physical, acid and construction parameters on the reduction of fracture pressure in a sandstone reservoir. The basic reservoir and perforation properties are given in Table 2. Rock constituents, relative contents and the initial radius

TABLE 2. Basic reservoir properties and perforation characteristics

Maximum horizontal principal stress, MPa	Minimum horizontal principal stress, MPa	Compressive strength, MPa	Young modulus,	Poisson's ratio MPa
85	64.8	267.2	35000	0.24
Formation temperature, °C	Perforation length, mm	Perforation diameter, mm	Perforation azimuth, °	Shot density, shoots/m
70	104.3	3.8	0	20

TABLE 3. Properties of rock constituents

Type	Mineral	$\rho_r$ (g/cm <sup>3</sup> )	Content(%)	$a_{0r}$ (cm)
I	Calcite	2.70	5.59	0.295
II	Plagioclase	2.68	5.49	0.293
III	Clay	2.65	24.22	0.630
IV	Quartz	2.43	63.64	1.048
V	Barite	4.12	1.06	0.037

of the hypothetical homogeneous mineral cylinder were given in Table 3.

Figure 8 shows how varying the acid concentration influences the damage variables with treatment time. Damage variables increase with treatment time for all acid concentrations. Because the 10 wt. % HCl pre-flush rapidly reacts with 5.59 wt. % calcite contained in the formation, the initial damage variable is 0.066. After 120 min of treatment, the three curves show damage variables of 0.1039, 0.1749 and 0.2391, corresponding, respectively, to increase the acid concentrations.

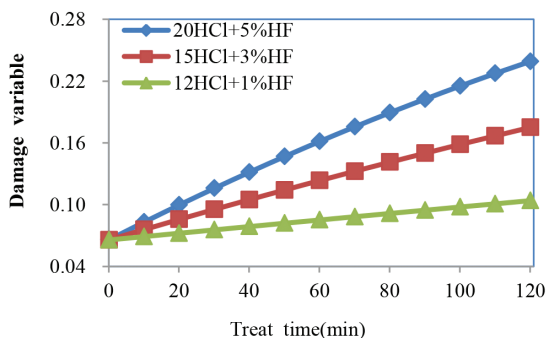


FIGURE 8. Effect of acid concentration on damage variables

Figure 9 shows the effect of temperature 50, 70, 90 and 110°C on damage variables, a given acid concentration of 15 wt. % HCl+3 wt. % HF. Damage variables increased with the formation temperatures, as the rate of mud acid-mineral reaction increases with the increasing temperature.

Figure 10 gives a prediction of fracture pressure reduction for different treatment times using an acid composition of 15 wt. % HCl+3 wt. % HF. After 120 min, the fracture pressure reduces by 5.0 MPa caused by the decrease of Young's modulus with acid damage (blue curve in Figure 10), while a fracture pressure reduction of

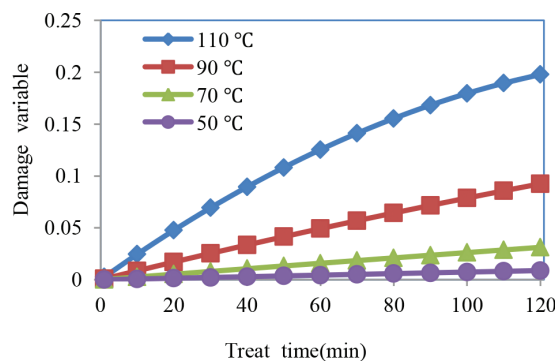


FIGURE 9. Effect of temperature on damage variables

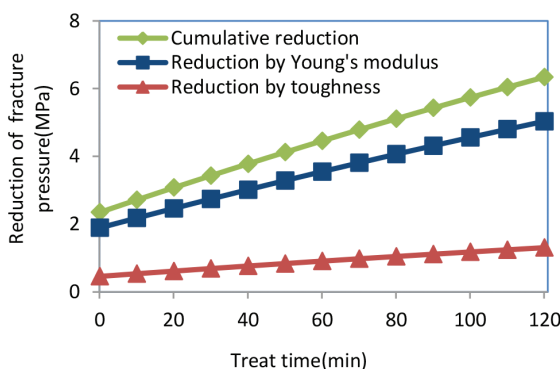


FIGURE 10. Effect of Young's modulus and Critical stress intensity on fracture pressure

1.5 MPa was observed, red curve, due to the decrease of critical stress intensity factor with acid damage after the same period of time. The pink curve shows the cumulative reduction of fracture pressure is 6.5 MPa due to Young's modulus and the Critical stress intensity, after 120 min of treatment time. Since the original predicted fracture pressure was 105.3 MPa using FEM, the fracture pressure after the acid damage was reduced to 98.8 MPa (=105.3

MPa- 6.5 MPa). This result gave a good match with the field data of 100 MPa, which confirming the reliability of the presented model.

#### CONCLUSION

In this study, acid damage on the sandstone rock samples mechanical properties and fracturing pressure in perforated wells were systematically investigated. The results can be summarized as follows:

Acid damage was an effective treatment method to reduce the fracture pressure in sandstone reservoirs. Based on the experimental study about the acid sensitivity of mineral particles and cementing materials, it was possible to establish a reasonable mechanism to explain the reduction of fracture pressure and how acid damage destroys the crystal structure of mineral particles, breaks the crystalline layers of the cementing materials, increased rock porosity and reduced rock strength.

A model that quantitatively predicts fracture pressure with acid damage was established by the combination of damage mechanics, fracturing mechanics and finite element theory, considering the effects of mineral constitution, acid composition, acid amount and formation temperature. The calculated results showed that it was possible to reduce fracture pressure with increasing acid concentration, temperature and treatment time.

#### ACKNOWLEDGEMENTS

The work was funded by the following: project (No. 51525404; No. 51504203; No. 51374178) supported by the National Natural Science Foundation of China, project (2015072) supported by the special fund of China's Central Government for the development of local colleges and universities, project (No.2014QHZ004) supported by scientific research starting project of SWPU, project (No.2014PYZ002) supported by scientific research starting project of SWPU and project (szjj2015-020) was supported by the open research subject of key laboratory of fluid power machinery and the Ministry of Education.

#### REFERENCES

- Anderson, R.A., Ingram, D.S. & Zanier, A.M. 1973. Determining fracture pressure gradients from well logs. *Journal of Petroleum Technology* 25: 1259-1268.
- Asadpourea, A., Mohammadib, S. & Vafaia, A. 2006. Modeling crack in orthotropic media using a coupled finite element and partition of unity methods. *Finite Elements in Analysis and Design* 42: 1165-1175.
- Atkinson, B.K. 1979. A fracture mechanics study of subcritical tensile cracking of quartz in wet environments. *Pure and Applied Geophysics* 117: 1011-1024.
- Colback, P.S.B. & Wild, B.L. 1965. The influence of moisture content on the compressive strength of rock. *Proceedings of the 3rd Canadian Rock Mechanics Symposium*. pp. 65-83.
- Chen, Z.X., Mian, C. & Yan, J. 1997. Determination of rock fracture toughness with hydraulic fracturing method. *Chinese Journal of Rock Mechanics and Engineering* 16: 59-62.
- Ding, W.X. & Feng, X.T. 2005. Study on chemical damage effect and quantitative analysis method of meso-structure of limestone. *Chinese Journal of Rock Mechanics and Engineering* 24: 1283-1288.
- Eaton, B.A. 1969. Fracture gradient prediction and its application in oilfield operations. *SPE Journal of Petroleum Technology* 21(10): 1353-1360.
- Feng, X.T., Chen, S. & Li, S. 2001. Effects of water chemistry on micro cracking and compressive strength of granite. *International Journal of Rock Mechanics & Mining Sciences* 38: 557-568.
- Fogler, H.S. 1975. Acidization II-the kinetics of the dissolution of sodium and potassium feldspar in HF/HCl acid mixtures. *Chemical Engineering Science* 30: 1325-1322.
- Freiman, S.W. 1984. Effects of chemical environments on slow crack growth in glasses and ceramics. *Journal of Geophysical Research* 89: 4072-4076.
- Haimson, B. & Fairhurst, C. 1967. Initiation and extension of hydraulic fractures in rocks. *Old SPE Journal* 7: 310-318.
- Hawkins, A.B. & McConnell, B.J. 1992. Sensitivity of sandstone strength and deformability to changes in moisture content. *Quarterly Journal of Engineering Geology* 25: 115-130.
- Higgs, N. 1981. Mechanical Properties of Ultrafine Quartz, Chlorite, Bentonite in Environments of the Upper Crust. Ph.D. dissertation, Texas A & M University, College Station, TX. (Unpublished).
- Hill, A.D. 1981. Theoretical and experimental studies of sandstone acidizing. *SPEJ* 21: 30-42.
- Hoshino, K. 1974. Effect of porosity on the strength of the classic sedimentary rocks. *Proceedings, Congress of the International Society for Rock Mechanics*. Advances in Rock Mechanics, Reports of Current Research, Part A. U. S. Committee on Rock Mechanics, National Academy of Sciences, Washington, D.C. 2: 511-516.
- Hossain, M.M., Rahman, M.K. & Sheik, S.R. 1999. A comprehensive monograph for hydraulic fracture initiation from deviated wellbores under arbitrary stress regimes. *SPE Asia Pacific Oil and Gas Conference and Exhibition*, 20-22 April, Jakarta, Indonesia.
- Huang, R.Z. & Xu, J.J. 1986. A new method to predict fracture pressure. *Oil Drilling & Production Technology* 3: 1-14.
- Hu, Y., Zhao, J., Zeng, Q., Xu, S. & Xie, H. 2003. Finite element method to calculate fracturing pressure of perforated well hydrofrac. *Natural Gas Industry* 23: 58-59.
- Kline, W.E. & Fogler, H.S. 1981. Dissolution kinetics: The nature of the particle attack of layered silicates in HF. *Chemical Engineering Science* 36: 871-879.
- Kronenberg, A.K. 1994. Hydrogen speciation and chemical weakening of quartz. In *Silica: Physical Behavior, Geochemistry and Materials Applications*, edited by Heaney, P.J., Prewitt, C.T. & Gibbs, G.V. *Mineralogical Society of America* 29: 123-176.
- Lemaitre, J. 1972. Evaluation of dissipation and damage in metals submitted to dynamic loading, mechanical behavior of materials. *Proceedings of the First International Conference*, Kyoto, Japan. pp. 540-549.
- Niemeijer, A.R. & Lloyd, G.E. 2010. The nature and importance of phyllonite development in crustal-scale fault cores: An example from the Median Tectonic Line, Japan. *Journal of Structural Geology* 28: 220-235.

- Rajesh, K.N. & Rao, B.N. 2010. Two-dimensional analysis of anisotropic crack problems using coupled mesh less and fractal finite element method. *International Journal of Fracture* 164: 285-318.
- Sibson, R.H. 1977. Fault rocks and fault mechanisms. *Journal of the Geological Society of London* 133: 140-213.
- Stephen, R.D. 1982. Prediction of fracture pressures for wildcat wells. *Journal of Petroleum Technology* 34: 863-872.
- Tang, L.S., Peng, C.Z. & Si, J.W. 2002. Testing study on effects of chemical action on crack propagation in rock. *Chinese Journal of Rock Mechanics and Engineering* 6: 822-827.
- Wiederhorn, S.M. & Johnson, H. 1973. Effect of electrolyte pH on crack propagation in glass. *Journal of the American Ceramic Society* 56: 192-197.
- William, E., Kline, H. & Scott, F. 1981. Dissolution of silicate minerals by hydrofluoric acid. *Industrial & Engineering Chemistry Fundamentals* 20: 155-161.

State Key Laboratory of Oil and Gas Geology and Exploration  
Southwest Petroleum University  
610500 Chengdu  
P.R. China

\*Corresponding author, email: zengfanhui023024@126.com

Received: 13 June 2013  
Accepted: 4 August 2015